Available online at www.sciencedirect.com

SciVerse ScienceDirect

Journal of Nutritional Biochemistry 23 (2012) 994–1006

Journal of Nutritional Biochemistry

Stimulation of GSH synthesis to prevent oxidative stress-induced apoptosis by hydroxytyrosol in human retinal pigment epithelial cells: activation of Nrf2 and JNK-p62/SQSTM1 pathways

Xuan Zou[a,b], Zhihui Feng[c,d], Yuan Li[d], Ying Wang[e], Karin Wertz[e], Peter Weber[e], Yan Fu[a,b], Jiankang Liu[d,*]

[a]College of Animal Sciences, Zhejiang University, Hangzhou, China
[b]Zhejiang California International NanoSystems Institute, Zhejiang University, Hangzhou, China
[c]Institute for Nutritional Sciences, Shanghai Institutes of Biological Sciences, Chinese Academy of Sciences, Shanghai; Graduate School of the Chinese Academy of Sciences, Beijing, China; Xi'an, China
[d]Institute of Mitochondrial Biology and Medicine, The Key Laboratory of Biomedical Information Engineering of Ministry of Education, Xi'an Jiaotong University School of Life Science and Technology, Xi'an, China
[e]DSM Nutritional Products, Inc., Basel, Switzerland

Received 2 October 2010; received in revised form 15 May 2011; accepted 16 May 2011

Abstract

The Nrf2-Keap1 pathway is believed to be a critical regulator of the phase II defense system against oxidative stress. By activation of Nrf2, cytoprotective genes such as heme oxygenase-1 (HO-1), NAD(P)H:quinone oxidoreductase (NQO-1) and γ-glutamyl-cysteine ligase (GCL) are induced. GCL-induced glutathione (GSH) production is believed to affect redox signaling, cell proliferation and death. We here report that *tert*-butyl hydroperoxide (*t*-BHP)-induced GSH reduction led to mitochondrial membrane potential loss and apoptosis in cultured human retinal pigment epithelial cells from the ARPE-19 cell line. Hydroxytyrosol (HT), a natural phytochemical from olive leaves and oil, was found to induce phase II enzymes and GSH, thus protect *t*-BHP-induced mitochondrial dysfunction and apoptosis. Depletion of GSH by buthionine-[*S*,*R*]-sulfoximine enhanced *t*-BHP toxicity and abolished HT protection. Overexpression of Nrf2 increased GSH content and efficiently protected *t*-BHP-induced mitochondrial membrane potential loss. Meanwhile, HT-induced GSH enhancement and induction of Nrf2 target gene (GCLc, GCLm, HO-1, NQO-1) messenger RNA (mRNA) were inhibited by Nrf2 knockdown, suggesting that HT increases GSH through Nrf2 activation. In addition, we found that HT was able to activate the PI3/Akt and mTOR/p70S6-kinase pathways, both of which contribute to survival signaling in stressed cells. However, the effect of HT was not inhibited by the PI3K inhibitor LY294002. Rather, c-Jun N-terminal kinase (JNK) activation was found to induce p62/SQSTM1 expression, which is involved in Nrf2 activation. Our study demonstrates that Nrf2 activation induced by the JNK pathway plays an essential role in the mechanism behind HT's strengthening of the antiapoptotic actions of the endogenous antioxidant system.

Keywords: Heme oxygenase-1 (HO-1); NAD(P)H:quinone oxidoreductase (NQO-1); γ-Glutamyl-cysteine ligase (GCL); Buthionine-[*S*,*R*]-sulfoximine (BSO); *tert*-Butyl hydroperoxide (*t*-BHP); Mitochondrial function

1. Introduction

Nuclear factor (erythroid-derived-2)-like 2, also known as Nrf2, is a master regulator of the antioxidant response [1–3]. Under normal or unstressed conditions, Nrf2 is tethered in the cytoplasm by Keap1 [4,5]. Keap1 acts as a substrate adaptor protein for Cullin 3-based ubiquitination, which results in the degradation of Nrf2 [6,7]. Activation of Nrf2 requires its translocation into the nucleus, where it heterodimerizes with a small Maf protein and binds to the antioxidant response element in the upstream promoter region of many antioxidative genes [8]. Therefore, there are two ways to mediate Nrf2 activation. One is to up-regulate Nrf2 expression, and the second is to disrupt critical cysteine residues between Keap1 and Nrf2, thus setting Nrf2 free for translocation.

Several target genes have been identified, such as heme oxygenase-1 (HO-1) [9], NAD(P)H:quinone oxidoreductase (NQO-1) and γ-glutamyl-cysteine ligase (GCL) [10]. GCL is a heterodimer consisting of catalytic (GCLc) and modifier (GCLm) subunits, both of which are products of Nrf2 target genes. GCL has been extensively investigated for its ability to regulate the synthesis of glutathione (GSH), one of the most important antioxidants *in vivo*. Previous studies indicated that GSH plays a fundamental role in DNA synthesis and repair, protein synthesis, amino acid transport and enzyme activation, in addition to its role as antioxidant [11–13]. It is also essential for regulating the nitric oxide cycle [14], for enhancing lymphocyte proliferation [15,16] and for regulating apoptosis. In consequence, GSH has been found to be widely involved in the

* Corresponding author. Institute of Mitochondrial Biology and Medicine, Xi'an Jiaotong University School of Life Science and Technology, Xi'an 710049, China. Tel.: +86 29 82665849.
E-mail address: j.liu@mail.xjtu.edu.cn (J. Liu).

0955-2863/$ - see front matter © 2012 Elsevier Inc. All rights reserved.
doi:10.1016/j.jnutbio.2011.05.006

etiology of several human diseases including cancer, neurodegeneration, obesity and diabetes.

p62/SQSTM1 (p62) was originally identified because it bound to the tyrosine kinase Lck [17]. Subsequently, it was found to bind atypical protein kinase C and act as a scaffold or adaptor protein in nuclear factor κB signaling pathways [18,19]. p62 has been reported to possess dual-binding sites for ubiquitin chains and LC3 and to be involved in autophagic clearance of ubiquitin aggregates [20]. Recent studies reported that up-regulation of endogenous p62 induced by a deficiency in autophagic function or by ectopic expression of p62 causes p62 to sequester Keap1 into aggregates through direct interaction between these two proteins; the resulting suppression of Nrf2 ubiquitination leads to increased Nrf2 stability and downstream gene activation [21,22]. Furthermore, p62 has been identified as an Nrf2 target gene. It is induced by oxidative stress mediated by Nrf2, and at the same time, p62 protein contributes to the activation of Nrf2, creating a positive feedback loop [23].

In previous studies, we reported that hydroxytyrosol (HT), a natural phytochemical from olive oil, activates Nrf2, induces target gene expression and therefore protects ARPE-19 cells from acrolein-induced cell death [24,25]. However, the acrolein treatment was acute and caused cell death by necrosis [26], and there has been little research into HT's effect on ARPE-19 cell apoptosis. In the current study, we found that a 6-h treatment with *tert*-butyl hydroperoxide (*t*-BHP) decreased GSH content and mitochondrial membrane potential (MMP), which are primary elements for triggering apoptosis; a 24-h treatment caused reactive oxygen species (ROS) production and oxidative damage. HT pretreatment efficiently blocked *t*-BHP-induced apoptosis through GSH enhancement. Using small interference RNA (siRNA) and a wild-type Nrf2 plasmid, we demonstrated that HT mediates GSH expression through Nrf2 activation. We also found that neither the PI3/Akt nor the mTOR/p70S6-kinase pathway is responsible for the Nrf2 activation, although HT activates both of them. Instead, c-Jun N-terminal kinase (JNK) activation was found to be involved in the regulation of GSH production. Although neither NQO-1 nor HO-1 is regulated by JNK activation, p62 — both a newly discovered Nrf2 target gene and Nrf2 inducer — was found to be regulated by JNK activation, providing a possible link between p62 and GSH production.

2. Materials and methods

2.1. Chemicals

t-BHP, SP600125, SB203580, monodansylcadaverine (MDC) and L-buthionine-sulfoximine (BSO) were purchased from Sigma (St. Louis, MO, USA); Lysotracker and DCF-DA were from Invitrogen (Carlsbad, CA, USA); LY294002 was from Cell Signaling Technology (Danvers, MA, USA); U0126 was from Santa Cruz Biotechnology (Santa Cruz, CA, USA); antibodies against NQO1, Atg12, Atg7, Atg3, Beclin-1 and LC3B were from Cell Signaling Technology; anti-Nrf2 and HO-1 were from Santa Cruz Biotechnology and anti-GCL was from NeoMarkers (Fremont, CA, USA). HT was provided by DSM Nutritional Products, Inc. (Basel, Switzerland).

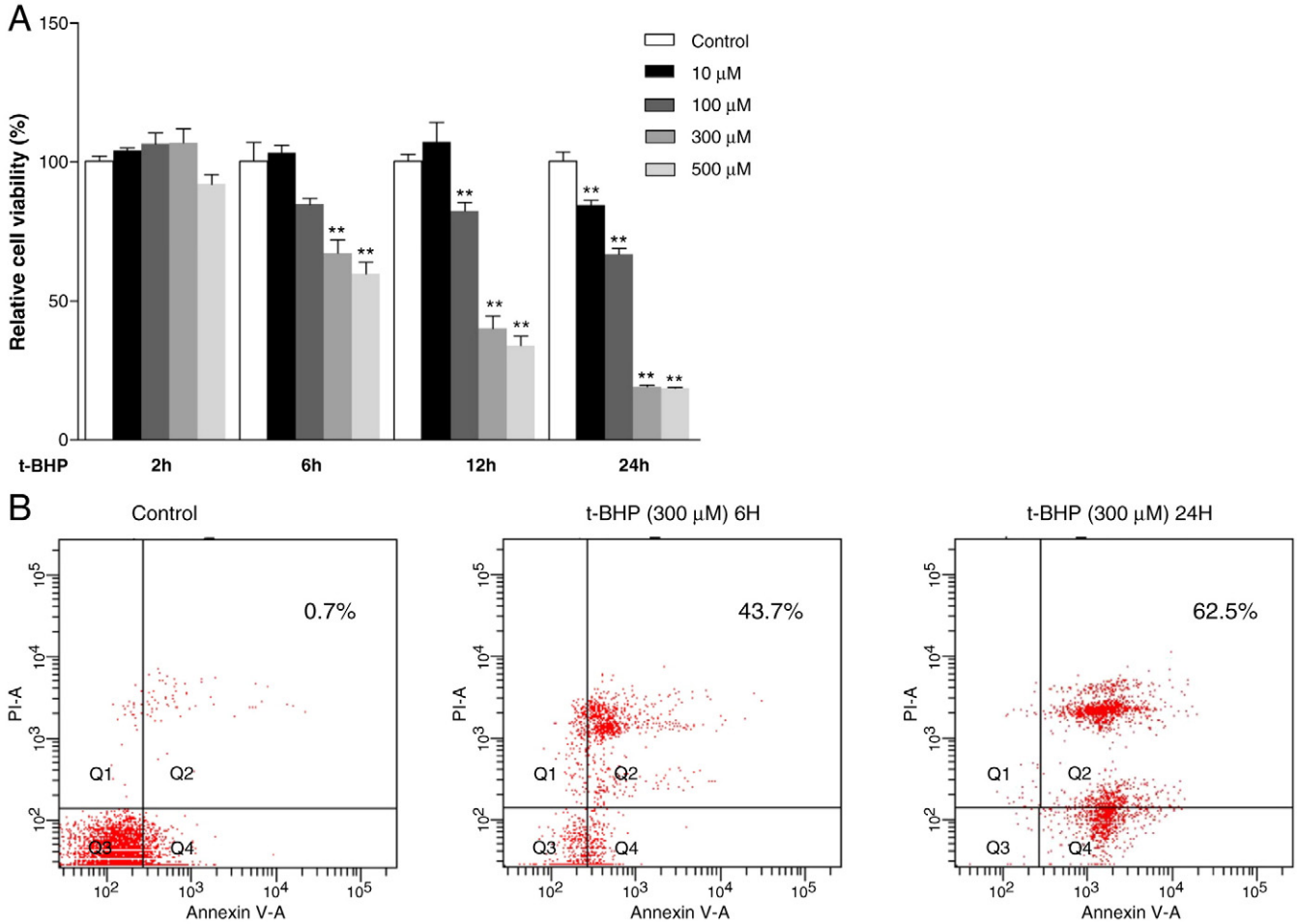

Fig. 1. *t*-BHP induces apoptotic cell death in ARPE-19 cells. (A) ARPE-19 cells were treated with *t*-BHP at the indicated concentrations (10, 100, 300, 500 μM) for 2, 6, 12 or 24 h and cell death was analyzed using the MTT method. (B) Cells were treated with 300 μM *t*-BHP for 6 or 24 h; the percentage of apoptotic cells was detected by Annexin V/PI dual staining with flow cytometry. For the MTT assay, values are means±S.E.M. from three separate experiments. *$P<.05$, **$P<.01$ versus control.

2.2. Cell culture

A human ARPE-19 cell line was obtained from Dr. Nancy J. Philp and was cultured in Dulbecco's modified eagle medium: nutrient mixture F-12 medium supplemented with 10% fetal bovine serum, 0.348% sodium bicarbonate, 2 mM L-glutamine, 100 U/ml penicillin and 100 μg/ml streptomycin [27]. Cell cultures were maintained at 37°C in a humidified atmosphere of 95% air and 5% CO_2. Medium was changed every 2 days. ARPE-19 cells were used within 10 generations.

2.3. MDC and lysotracker staining

ARPE cells were seeded in 6-well plates for 24 h, when they typically had reached 80% confluency. MDC and lysotracker staining were performed according to the manufacturers' instructions and were visualized using an Olympus IX-71 fluorescence microscope.

2.4. MTT assay for cell viability

ARPE-19 cells were seeded in 96-well plates at a density of 4×10^4 per well for 24 h. Cells were treated with different concentrations of *t*-BHP or HT for the indicated time periods. The number of viable cells was then determined by the addition of MTT (3-[4,5-dimethylthiazol-2-yl]-2,5-diphenyltetrazolium bromide). Optical densities were read at 555 nm using a microplate spectrophotometer (Multiskan Ascent; Thermo Fisher Scientific Inc. Waltham, MA, USA).

2.5. JC-1 assay for MMP

MMP ($\Delta\Psi$) was assessed in live ARPE-19 cells using the lipophilic cationic probe 5,5′,6,6′-tetrachloro-1,1′,3,3′-tetraethyl-benzimidazolyl-carbocyanine iodide (JC-1). For quantitative fluorescence measurements, cells were rinsed once after JC-1 staining and scanned with a microplate fluorometer (Fluoroskan Ascent; Thermo Fisher Scientific Inc.) at 488-nm excitation and 535- and 590-nm emission, to measure green and red JC-1 fluorescence, respectively. Each well was scanned by measuring the intensity of each of 25 squares (of 1-mm^2 area) arranged in a 5×5 rectangular array.

2.6. Assays for the activities of mitochondrial complexes

Reduced nicotinamide adenine dinucleotide (NADH)-ubiquinone reductase (complex I), succinate-CoQ oxidoreductase (complex II), ubiquinol cytochrome c reductase (complex III) and Mg^{2+}-ATPase (complex V) were measured spectrometrically using conventional assays as described [28,29].

2.7. Assay for oxygen consumption capacity

Oxygen consumption capacity was determined with the BD Oxygen Biosensor System (BD Biosciences). Plates were sealed and scanned by a fluorescence spectrometer (Fluoroskan Ascent, Thermo Fisher Scientific Inc.) at 1-min intervals for 60 min at an excitation wavelength of 485 nm and emission wavelength of 630 nm.

2.8. Intracellular adenosine 5′-triphosphate (ATP) level measurement

Cells were cultured in 6-well plates. After treatment, cells were lysed by 0.5% Triton X-100, in 100 mM glycine buffer, pH 7.4. Intracellular ATP level assays were carried out with an ATP bioluminescent assay kit (Sigma). ATP is consumed and light is emitted when firefly luciferase catalyzes the oxidation of D-luciferin [30].

2.9. Determination of ROS generation

The generation of intracellular ROS was determined by fluorescence of 2′,7′-dichlorofluorescein (DCF-DA), upon oxidation of nonfluorescent, reduced, DCFH [31]. The fluorescence intensity of the supernatant was measured with a microplate fluorometer (Fluoroskan Ascent; Thermo Fisher Scientific Inc.) at 488-nm excitation

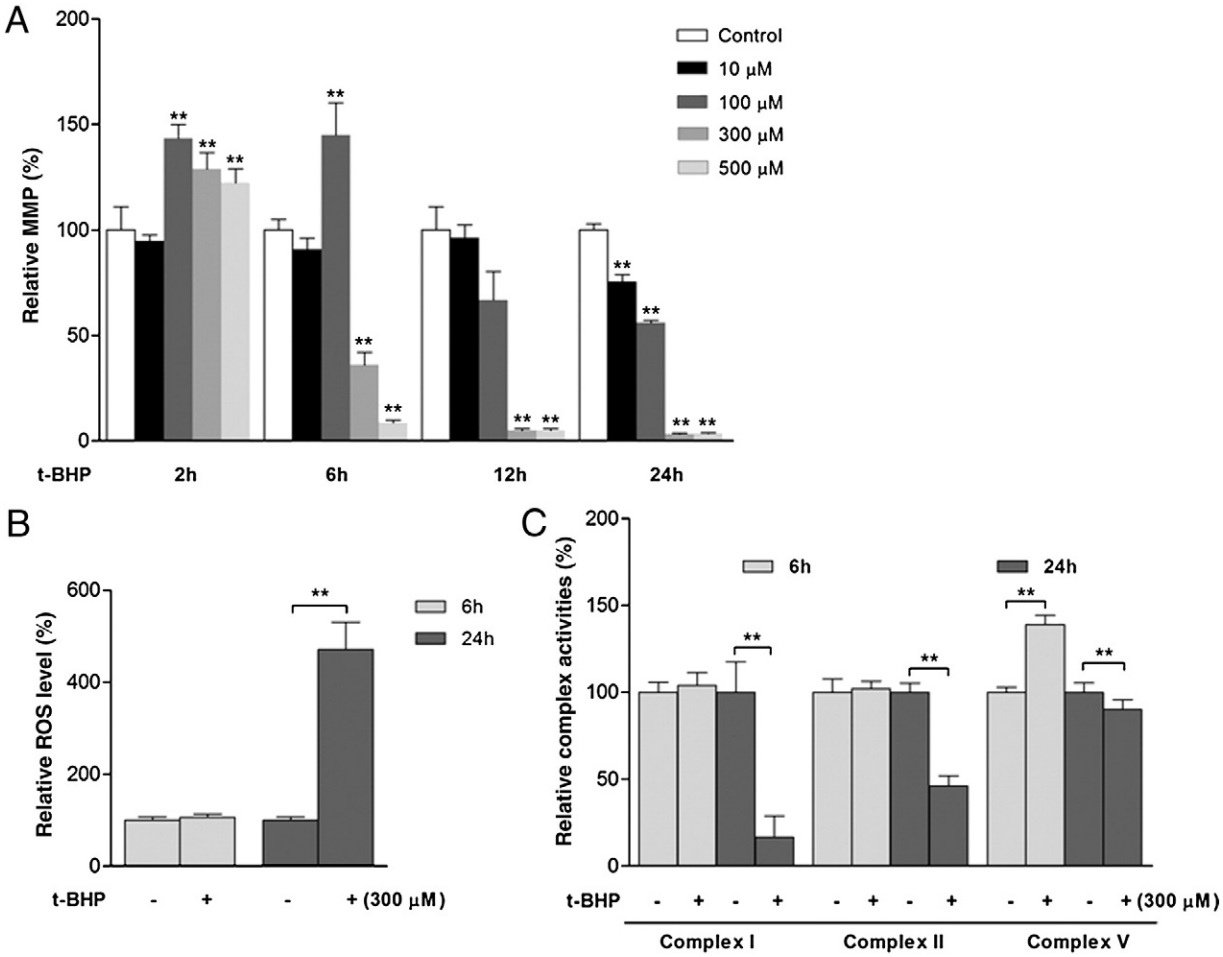

Fig. 2. Effects of *t*-BHP on oxidative stress and mitochondrial function. (A) ARPE-19 cells were treated with *t*-BHP at the indicated concentrations (10, 100, 300, 500 μM) for 2, 6, 12 or 24 h, and cellular MMP was detected with the JC-1 probe. (B) Cells were treated with 300 μM *t*-BHP for 6 or 24 h; ROS levels were detected with DCF-DA. (C) Mitochondria were isolated, and complex I, II, and V activities were measured. Values are means±S.E.M. from three separate experiments. *P<.05, **P<.01 versus related control.

and 535-nm emission. Cellular oxidant levels were expressed as relative DCF fluorescence per microgram of protein (BCA method).

2.10. Intracellular GSH measurement

GSH levels were measured with 2,3-naphthalenedicarboxyaldehyde (NDA) by a published method [32]. A 20 μl sample and 180 μl of NDA derivatization solution [50 mM Tris (pH 10), 0.5 N NaOH and 10 mM NDA in Me_2SO, vol/vol/vol 1.4:0.2:0.2] were added to each well of a 96-well plate. The plate was covered to protect the wells from room light and allowed to incubate at room temperature for 30 min. The NDA–GSH fluorescence intensity was measured (472 ex/528 em) with a microplate fluorometer (Fluoroskan Ascent; Thermo Fisher Scientific Inc.).

2.11. siRNA transfection

Transfection with Nrf2 siRNA was performed using the target sequence 5′–3′ for human Nrf2 siRNA. ARPE-19 cells were seeded at 1.5×10^5 cells per well in 6-well plates for transfection, Western blot and real-time polymerase chain reaction (PCR) assays. The transfection, using Lipofectamine 2000, was performed as described in the supplier's manual. Briefly, appropriate amounts of Nrf2 siRNA and 5 μl Lipofectamine 2000 in 250 μl serum-free DMEM/12 medium were prepared in separate RNase-free tubes. After 5-min incubation, the siRNA and Lipofectamine were mixed and incubated for another 20 min and then added to each well. After 100 pmol siRNA per well for 24 h, cells were treated with HT 6 h for RNA analysis, or 24 h for protein analysis.

2.12. Overexpression of Nrf2

ARPE-19 cells were transiently transfected with pCDNA3-Myc3-Nrf2-FLAG (a gift from Dr. Yue Xiong, Lineberger Cancer Center, University of North Carolina at Chapel Hill, NC, USA) using Lipofectamine 2000. Cells were collected for Western blot and GSH measurements 24 h after transfection or treated for another 6 h with 300 μM *t*-BHP for detection of MMP.

2.13. Flow cytometric analysis

Apoptosis was determined by using the Annexin V–FITC (fluorescein isothiocyanate) apoptosis kit (Beyotime, Jiangsu, China) which detects cell surface changes that occur early in the apoptotic process. The assay was performed according to the manufacturer's instructions. After growth and treatment, the cells were collected and washed with phosphate-buffered saline; 1×10^5 cells were incubated with 200 μl Annexin V–FITC solution for 10 min at room temperature and with 200 μl propidium iodide (PI) solution for another 10 min. The samples were then analyzed by a FACScan flow cytometer (Becton Dickinson, Franklin Lakes, NJ, USA).

2.14. Real-time PCR

Total RNA was extracted from cells using TRIzol reagent (Invitrogen) according to the manufacturer's protocol. Reverse transcription was performed using PrimeScript RT-PCR Kit (TaKaRa, DaLian, China) followed by semiquantitative real-time PCR with specific primers. Primers were as follows: Nrf2, TTCAGCAGCATCCTCTCCACAG (forward)

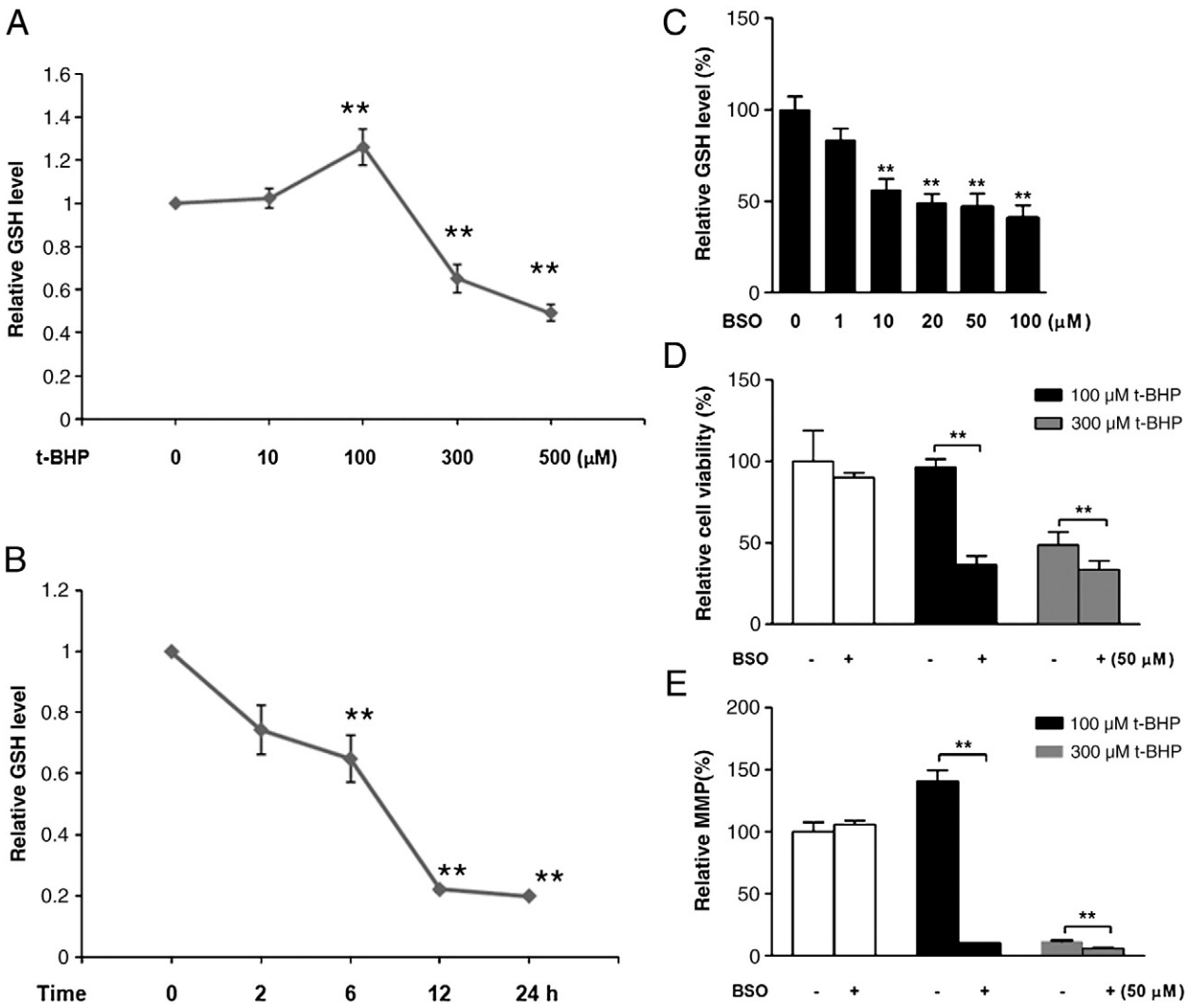

Fig. 3. Role of GSH during apoptosis. (A) Dose response of total GSH levels in ARPE-19 cells to 6-h treatments of 10, 100, 300 or 500 μM *t*-BHP: cells were harvested and cell lysates were assayed for total GSH. (B) Time response of total GSH levels in cells treated with 300 μM *t*-BHP for 2, 6, 12 or 24 h: cell lysate GSH levels were analyzed. (C) GSH levels of lysates from ARPE-19 cells treated with BSO (1, 10, 20, 50 or 100 μM) for 24 h. Viability determined by MTT (D), and MMP determined by JC-1 fluorescence (E) of cells pretreated with 50 μM BSO for 24 h, followed by 6-h exposure to 100 or 300 μM *t*-BHP in the absence of BSO. Values are means±S.E.M. from three separate experiments. *P<.05, **P<.01 versus related control.

and GCATGCTGTTGCTGATACTGG (reverse); p62, CTTGCGTCCCATGAGGTCTT (forward) andCCCATCCAGCAGGTTACAGC(reverse);GCLc,GGCGATGAGGTGGAATAC(forward)and AAAGGGTAGGATGGTTTGG(reverse);GCLm,ATCAAACTCTTCATCATCAAC(forward)and GATTAACTCCATCTTCAATAGG(reverse);NQO-1,TGGCTAGGTATCATTCAACTC(forward) and CCTTAGGGCAGGTAGATTCAG (reverse); HO-1, GCCAGCAACAAAGTGCAAGAT (forward) and GGTAAGGAAGCCAGCCAAGAG (reverse); β-actin, CCACACCTTCTACAAT-GAGC (forward) and GGTCTCAAACATGATCTGGG (reverse).

2.15. Western blot analyses

Samples were lysed with Western and IP lysis buffer (Beyotime, Jiangsu, China). The lysates were homogenized, and the homogenates were centrifuged at 13,000*g* for 15 min at 4°C. The supernatants were collected, and protein concentrations were determined with the BCA Protein Assay kit (Pierce 23225). Equal aliquots (20 μg) of protein samples were applied to 10% sodium dodecyl sulfate polyacrylamide gel electrophoresis (SDS-PAGE) gels, transferred to pure nitrocellulose membranes (PerkinElmer Life Sciences, Boston, MA, USA) and blocked with 5% nonfat milk. The membranes were incubated with anti-Nrf2, anti-p62, anti-HO-1, anti-Histone H1 (1:1000 Santa Cruz), anti-NQO1, anti-Atg12, anti-Atg7, anti-Atg3, anti-Beclin-1 and anti-LC3B (1:1000; Cell Signaling; 1:1000 Upstate), anti-GCL (1:1000; NeoMarkers) or anti-β-actin (1:10,000; Sigma) at 4°C overnight. Then the membranes were incubated with antirabbit or antimouse antibodies at room temperature for 1 h. Chemiluminescent detection was performed by an ECL Western blotting detection kit (Pierce). Nuclear and cytoplasmic Nrf2 were prepared with the Nuclear and Cytoplasmic Protein Extraction Kit (Beyotime Institute of Biotechnology, Shanghai, China) and analyzed by Western blot. The results were analyzed by Quantity One software to obtain the optical density ratio of target protein to β-actin.

2.16. Statistical analysis

Data are presented as means±S.E.M. Statistical significance was evaluated with one-way analysis of variance followed by least significant difference post hoc analysis. In all comparisons, the level of significance was set at $P<.05$.

3. Results

3.1. t-BHP apoptotic induction on ARPE-19 cell

To investigate the effect of *t*-BHP on cell survival, ARPE-19 cells were treated with *t*-BHP at 10, 100, 300 or 500 μM concentrations, each for 2, 6, 12 or 24 h. *t*-BHP began to induce 30% cell death at 300 μM for 6 h (Fig. 1A); 500 μM produced a similar effect. We used a 300-μM treatment for the following tests.

The cell death process induced by *t*-BHP was measured by Annexin-V/PI staining and flow cytometry. Treatment with 300 μM *t*-BHP for 6 h induced late apoptosis in 43.7% of cells, while 24-h treatment induced 62.5% (Fig. 1B), indicating that apoptosis is the major death process induced by *t*-BHP.

3.2. MMP loss in the induction of apoptosis

Mitochondria are the predominant sources of cellular energy and also play a major part in the progression of apoptosis. We investigated MMP status as a function of *t*-BHP challenge time and dose. Instead of a reduction, MMP was increased by a 2-h exposure to 100, 300 or 500 μM *t*-BHP. At 6 h, both 300- and 500-μM doses caused a greater than 50% loss of MMP, while after 24 h, even 10 μM *t*-BHP decreased MMP significantly (Fig. 2A).

We then tested whether oxidative damage was the cause of MMP loss by measuring ROS production. There was no increase in

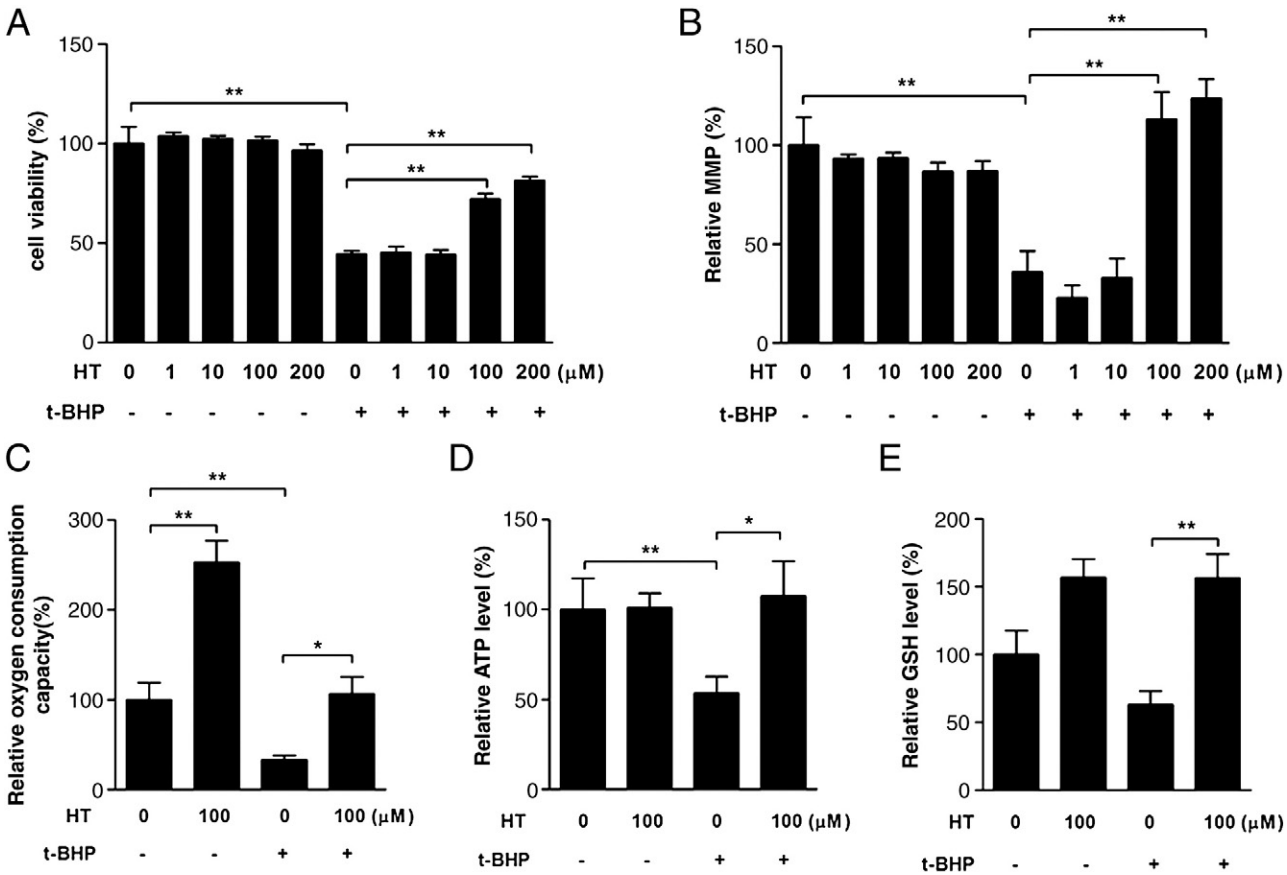

Fig. 4. HT protects *t*-BHP-induced cell death and mitochondrial function. ARPE-19 cells were pretreated with the indicated concentrations of HT (1, 10, 100, 200 μM) for 24 h, followed by a 6-h treatment with 300 μM *t*-BHP. Cell viability (A) and MMP (B) were analyzed. Cells were treated with 100 μM HT for 24 h, followed by a 6-h treatment with 300-μM *t*-BHP treatment in the absence of HT; cell oxygen consumption capacity (C), ATP contents (D) and GSH (E) contents were analyzed. Values are means±S.E.M. from three separate experiments. *$P<.05$, **$P<.01$ versus related control.

ROS levels associated with a 6-h treatment of 300 μM *t*-BHP, while treatment for 24 h produced a more than fourfold increase (Fig. 2B). Next, we isolated mitochondria and tested mitochondrial complex I, II and V activities. Similar to the ROS results, the 6-h 300-μM treatments affected the activity only of complex V, and neither of the others. After 24 h of treatment, all the complex activities decreased (Fig. 2C). These results indicate that oxidative damage was not responsible for the MMP loss since after 6 h, there was no obvious oxidative damage, but more than 50% of the MMP was lost. This gave us a clue that the loss of MMP induced by *t*-BHP may induce apoptosis directly.

3.3. GSH content is critical for maintaining MMP during apoptosis

We investigated changes in GSH during *t*-BHP challenge and whether GSH content affects MMP and apoptosis. We treated ARPE-19 cells with *t*-BHP for 6 h at different doses and found that both 300 and 500 μM concentrations reduced GSH contents, while there was a small increase with the 100-μM treatment (Fig. 3A). Moreover, the longer cells were exposed to 300 μM *t*-BHP, the lower GSH levels fell (Fig. 3B). BSO, a specific inhibitor of GSH synthesis, was found significantly inhibiting GSH production from 10 to 100 μM (Fig. 3C). We have chosen the middle dose of 50 μM

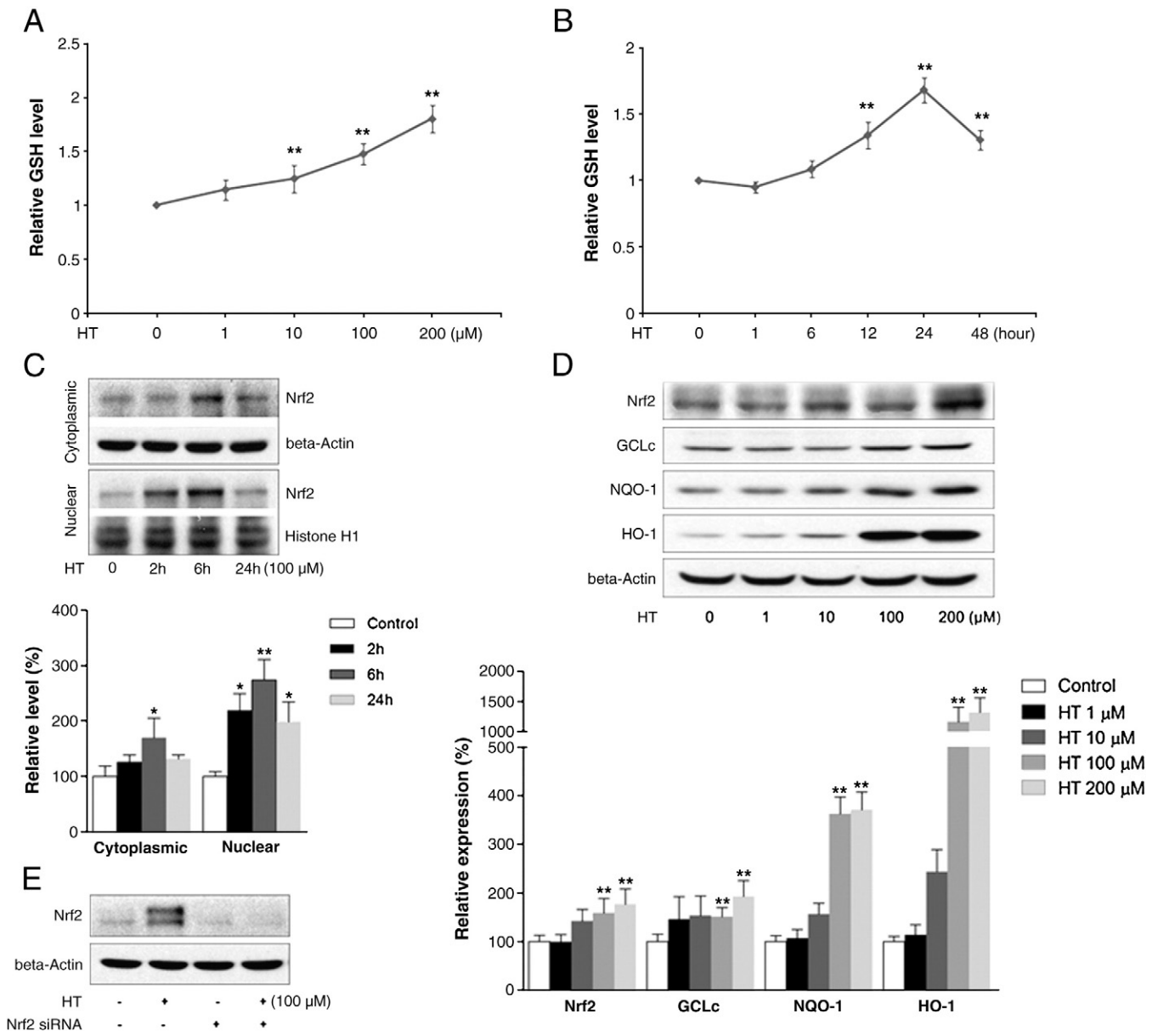

Fig. 5. HT induces GSH production by Nrf2 activation. Total GSH levels were measured following HT treatment of ARPE-19 cells; cells were harvested and cell lysates were assayed. (A) Dose response: ARPE-19 cells were treated with 1, 10, 100 or 200 μM for 24 h. (B) Time response: cells were treated with 100 μM HT for 2, 6, 12 or 24 h. Nrf2 activation was determined by Western blot. (C) The cytoplasmic and nuclear parts of cells were separated and analyzed, following treatment with HT for 2, 6 or 24 h (upper panel: Western blot image; lower graph: relative image quantification). (D) Expression of Nrf2 target gene product proteins was determined by Western blot after treating cells with 1, 10, 100 or 200 μM HT for 24 h (upper panel: Western blot image; lower graph: relative image quantification). Effects of silencing Nrf2 by siRNA transfection were studied by protein and RNA analysis. Cells were transiently transfected with Nrf2 siRNA, 100 pmol per well in 6-well plates for 24 h, followed by treatment with 100 μM HT for 6 or 24 h. Nrf2 protein levels (E) and GSH contents (K) were detected after 24 h of HT treatment; Nrf2, GCLc, GCLm, HO-1 and NQO-1 mRNA levels were examined by real-time PCR after 6 h of HT treatment (F, G, H, I and J, respectively). Values are means±S.E.M. from three separate experiments. **P*<.05, ***P*<.01 versus related control.

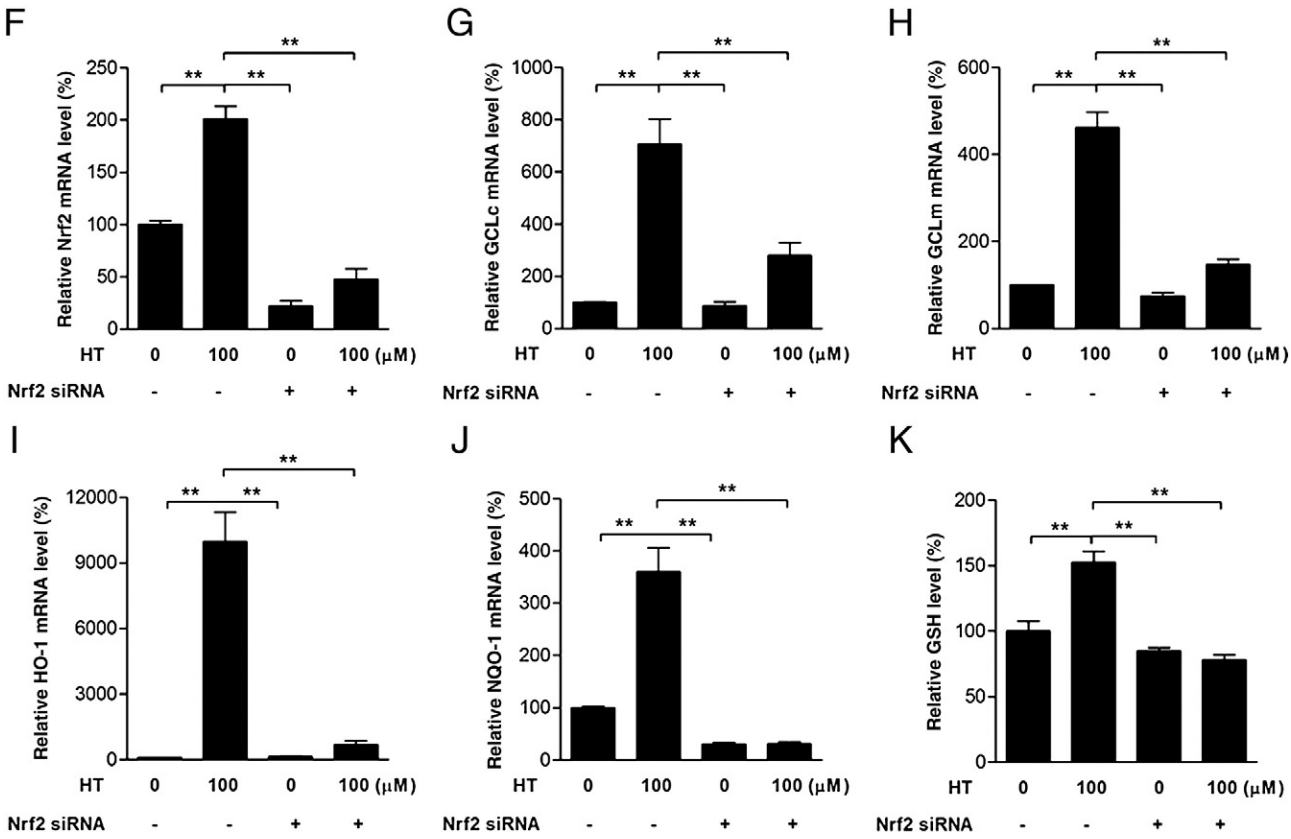

Fig. 5. (*continued*).

for getting more stable effect since no toxicity effect was found (data not shown). After 50-μM BSO treatment, cells were challenged with 100 or 300 μM *t*-BHP. Under normal conditions, cell death was not induced by 100 μM *t*-BHP. However, when pretreated with BSO, 100-μM *t*-BHP treatment caused more than 50% cell death (Fig. 3D). More surprisingly, pretreatment with BSO followed by 100-μM *t*-BHP treatment induced about 90% MMP loss, in contrast to a small increase in MMP in response to 100-μM *t*-BHP challenge without BSO pretreatment (Fig. 3E). Similar results were shown in response to 300 μM *t*-BHP with or without BSO pretreatment (Fig. 3D, E). BSO-only treatment had no effects on either cell viability or MMP. These results suggest that alteration of the intracellular GSH redox environment results in increased instability of MMP and sensitivity of cells to *t*-BHP challenge.

3.4. HT protects against mitochondrial dysfunction and cell death induced by t-BHP

In our previous study [24], HT exerted efficient protection of ARPE-19 cells against acrolein-induced acute cell death. In the present study, we tested how HT affects apoptosis. Cells were pretreated with HT at varying doses for 24 h, followed by treatment with 300 μM *t*-BHP for 6 h. Both 100 and 200 μM HT protected cells from *t*-BHP-induced cell death (Fig. 4A), and both these concentrations similarly restored MMP (Fig. 4B). Then we tested mitochondrial function, because it plays an important role in cell apoptosis. *t*-BHP induced a 50% reduction in mitochondrial oxygen consumption capacity and ATP level, while HT pretreatment restored these parameters to normal levels in cells challenged by *t*-BHP (Fig. 4C, D). HT pretreatment increased GSH by about 50% and protected against the decrease in GSH induced by a *t*-BHP challenge (Fig. 4E).

3.5. HT increases GSH levels through Nrf2 activation

In order to extend the GSH results, we investigated how HT affords protection by increasing GSH cell contents. We treated cells with HT and found that GSH contents increase as a function of both time and dose (Fig. 5A, B). Then we measured both cytoplasmic and nuclear levels of Nrf2, a transcription factor that is responsible for GSH production upon translocation from the cytoplasm into the nucleus. The theoretical MW of Nrf2 is about 57 kDa for human, mice and rats. However, Nrf2 is a polyubiquitation protein *in vivo*. It has been noted that the apparent molecular weight of human or murine Nrf2 in SDS-PAGE ranges from 57 to 110 kDa. Both N- and C-Santa Cruz antibodies recognize a cluster of significantly increased bands at 100 kDa with overexpressed Nrf2 or dominate negative Nrf2 as controls [33]. Thus, in our study, we mainly detected 100 kDa Nrf2. As shown in Fig. 5C, HT induced Nrf2 translocation even after treatment of only 2 h. After a 24-h treatment, expressions of Nrf2 and some of its target genes products proteins were examined. Results showed that expression levels of Nrf2, GCLc, NQO-1 and HO-1 were significantly induced by HT at both 100 and 200 μM concentrations (Fig. 5D). To determine whether Nrf2 was the critical regulator for HT-induced GSH production, we cultured cells with siRNA specific for Nrf2 and found that HT failed to up-regulate Nrf2 expression when cells were treated in this way (Fig. 5E). For further confirmation, messenger RNA (mRNA) levels of Nrf2 and its target genes were examined. After ARPE-19 cells were transfected with Nrf2 siRNA for 24 h and cultured with HT for an additional 6 h, Nrf2 mRNA levels were found to be consistent with Nrf2 protein levels (Fig. 5F). Moreover, HT did not up-regulate mRNA levels of Nrf2 target genes including GCLc, GCLm, HO-1 and NQO-1 when Nrf2 was silenced (Fig. 5G-J). The increase in GSH contents induced by HT was

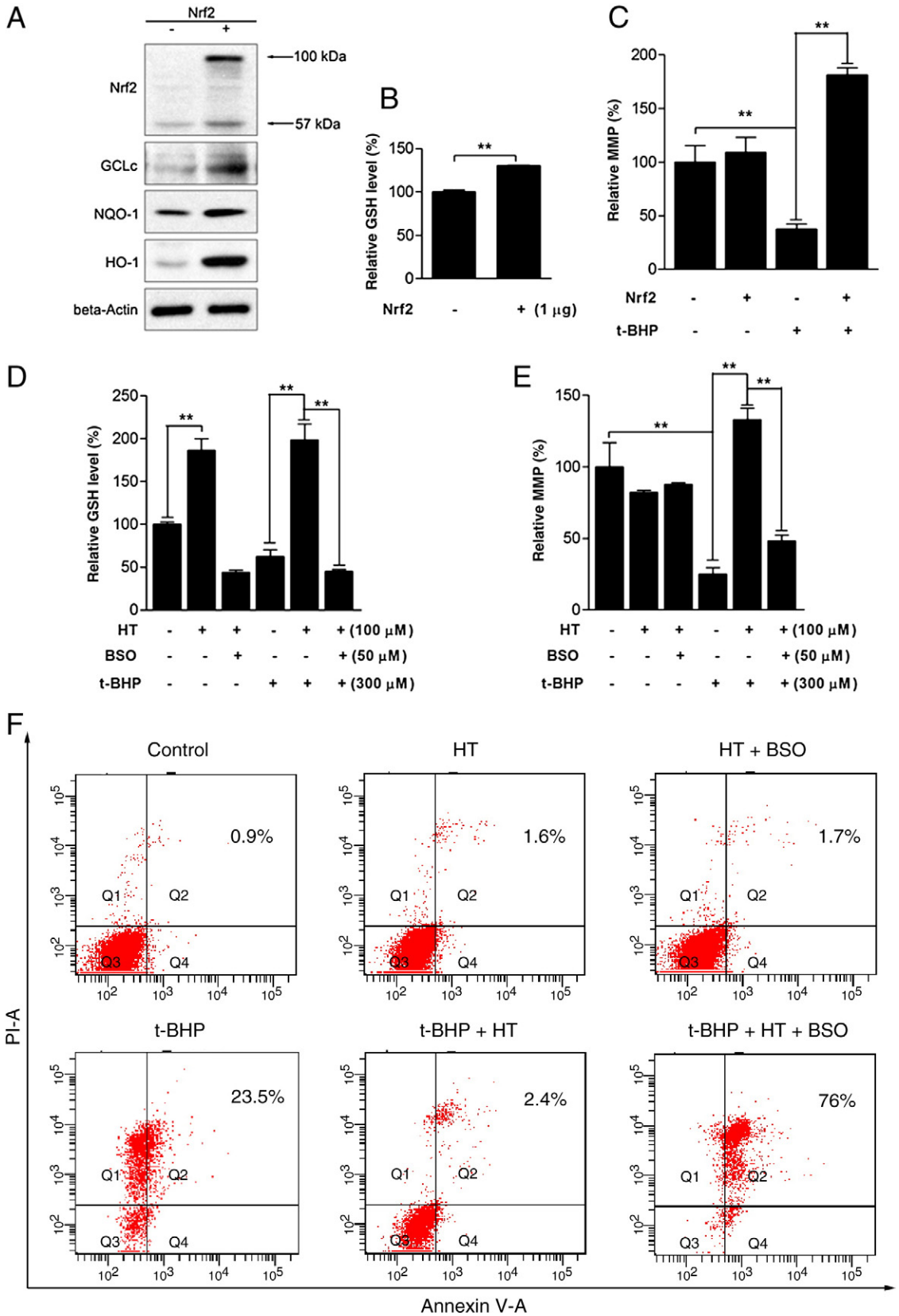

Fig. 6. HT protects *t*-BHP-induced apoptosis via GSH enhancement. Cells were transiently transfected with pCDNA3-Myc3-Nrf2 or empty vector, 1 μg per well in 6-well plates for 24 h. Nrf2, GCLc, NQO-1 and HO-1 protein expressions (A) and GSH contents (B) were measured after 24 h of transfection. (C) MMP was measured in cells transfected for 24 h, followed by a 6-h challenge with 300 μM *t*-BHP. Cells were pretreated with 100 μM HT with or without 50 μM BSO for 24 h, and followed by a 6-h challenge with *t*-BHP: GSH contents (D), MMP (E) and cell apoptosis (F) were examined. Values are means±S.E.M. from three separate experiments. *P<.05, **P<.01 versus related control.

also blocked by Nrf2 siRNA (Fig. 5K). These results lead us to conclude that HT induces GSH production by activation of Nrf2.

3.6. HT protects ARPE-19 cells through GSH enhancement

We hypothesized that GSH enhancement is the critical pathway that efficiently enables HT to protect against *t*-BHP-induced apoptosis. To verify this hypothesis, Nrf2 was overexpressed, and expression levels of GCLc, NQO-1 and HO-1 were examined (Fig. 6A). The GSH level was increased by Nrf2 overexpression (Fig. 6B). We challenged cells with *t*-BHP after transfecting with the Nrf2 construct. Nrf2 overexpression prevented *t*-BHP-induced MMP loss (Fig. 6C), which correlated with protection by HT. We then cultured cells for 24 h in the presence of HT and with BSO present or absent, and challenged them with 300 μM *t*-BHP for an additional 6 h. GSH contents and MMP status were measured. HT failed to increase GSH contents when cells were cultured with BSO, which decreased GSH contents by about 50%. When cells were challenged with *t*-BHP, HT was not able to increase GSH contents in the presence of BSO (Fig. 6D). The results for MMP were similar: HT failed to prevent *t*-BHP-induced MMP loss when cultured

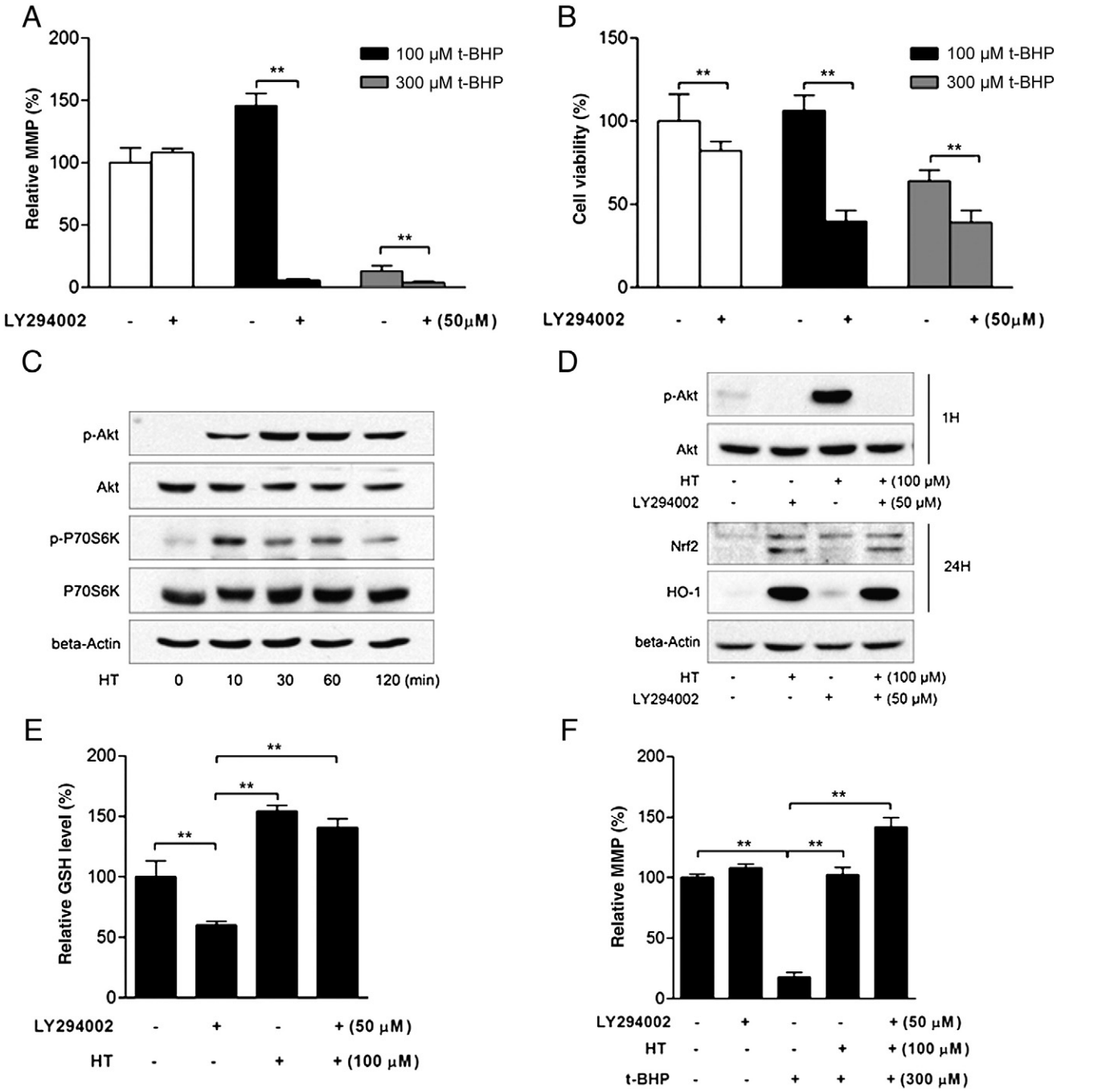

Fig. 7. Role of the PI3/Akt/mTOR/p70S6-kinase pathway in the induction of Nrf2. ARPE-19 cells were pretreated with 50 μM LY294002 for 24 h, followed by 100 or 300 μM *t*-BHP for another 6 h. MMP (A) and cell viability (B) were examined. (C) Cells were treated with 100 μM HT for 10, 30, 60 or 120 min, and Akt, p70S6K phosphorylation and expression were analyzed by Western blot. Cells were treated with 100 μM HT with or without LY294002 for 1 or 24 h: Akt phosphorylation and expression were analyzed after 1 h (D), Nrf2, HO-1 expression and GSH content (E) were analyzed after 24 h. (F) After treatment with HT and LY294002 for 24 h, cells were further challenged with 300 μM *t*-BHP, and MMP was examined. Values are means±S.E.M. from three separate experiments. **P*<.05, ***P*<.01 versus related control.

with BSO (Fig. 6E). This leads us to reason that MMP is correlated with the failure of GSH induction. We examined the effects of HT on *t*-BHP-induced cell apoptosis with or without BSO treatment. Annexin V/PI dual staining showed that HT or BSO treatment alone had no obvious effect on cell apoptosis and that *t*-BHP drove 23.5% of cells into apoptosis after a 6-h treatment (Fig. 6F). When cells were cultured with BSO, HT failed to inhibit *t*-BHP-induced cell apoptosis. Moreover, *t*-BHP challenge induced more cell apoptosis when cells were pretreated with BSO and HT (Fig. 6F). We conclude from these results that HT protects cells from *t*-BHP-induced apoptosis by increasing GSH levels.

3.7. Role of PI3/Akt/mTOR/p70S6-kinase pathway in Nrf2 induction by HT

The PI3/Akt/mTOR/p70S6-kinase pathway is part of survival signaling in cells confronted with stress, and many reports have shown that PI3/Akt pathway activation can induce Nrf2 activation and regulate antioxidant functions in cells [34–37]. It was our interest to reveal how ARPE-19 cells respond when challenged by *t*-BHP. Cells were incubated with the PI3/Akt pathway inhibitor LY294002 for 24 h and further treated with 100 or 300 μM *t*-BHP for 6 h. Alone, 100 μM *t*-BHP had no effect on cellular MMP or viability. Likewise, LY294002 treatment showed no effect on MMP, although it did decrease cell viability significantly (Fig. 7A, B). However, after pretreating with LY294002, 100 μM *t*-BHP was able to cause serious MMP loss and cell death (Fig. 7A, B). Similar results were observed after 300 μM *t*-BHP treatment. Since the PI3/Akt pathway is important to ARPE-19 cell survival, we then tested whether HT may induce Nrf2 activation via the PI3/Akt/mTOR/p70S6-kinase pathway. For this purpose, we treated cells with 100 μM HT for different time periods. HT activated the pathway for all periods between 10 min and 2 h (Fig. 7C). However, when cells were treated with both HT and LY294002 for 1 h, HT could not induce Akt phosphorylation. Surprisingly, even after a 24-h treatment with LY294002, HT still retained the capacity (1) to induce Nrf2 and HO-1 expression (Fig. 7D), (2) to induce GSH production (Fig. 7E) and (3) to prevent *t*-BHP-induced MMP loss (Fig. 7F). These results clearly show that activation of Nrf2 and induction of GSH production by HT are not regulated by the PI3/Akt/mTOR/p70S6-kinase pathway, despite its significance for cell survival.

3.8. HT-induced p62 expression is independent of autophagic dysfunction

It has been reported that p62 is involved in regulating the formation of protein aggregates and that it is removed by autophagy [20]. When autophagy is abolished, p62 accumulates in aggregates [38]. Recently, p62 has been reported to target Keap1 directly and to activate Nrf2 [22]. Thus, we wanted to determine whether HT might regulate p62 levels and whether autophagy is involved. We treated cells with HT for 6 and 24 h at the indicated concentrations and found that a 6-h treatment with HT dose-dependently increases p62 mRNA levels (Fig. 8A), while a 24-h treatment elevates p62 protein levels (Fig. 8B). However, staining with Lysotracker and MDC showed that treatment with HT for 24 h did not affect either lysosome or autophagosome numbers, respectively (Fig. 8C). Furthermore, Western blot results showed that none of the autophagy-related proteins Atg12, Atg7, Beclin-1, Atg3 and LC3B were affected by HT treatment (Fig. 8D). Hence, the HT-induced increase in p62 levels in ARPE-19 cells is independent of autophagic deficiency.

3.9. Involvement of the JNK pathway in p62, GSH induction and cell survival

As demonstrated above, the mechanism by which HT protects cells from *t*-BHP-induced apoptosis does not involve the PI3/Akt/mTOR/p70S6-kinase pathway. This raises the question whether the mitogen-activated protein kinases (MAPK) pathway may be involved. In the absence of 100 μM HT, we treated cells with three MAPK inhibitors: 10 μM SP600125 for c-Jun N-terminal kinase (JNK), 10 μM U0126 for extracellular signal-regulated kinase 1/2 (Erk1/2) and 20 μM SB203580 for p38. After 24 h, both GSH and p62 levels were found decreased after JNK inhibitor treatment (Fig. 9A, C). Furthermore, in the presence of HT treatment, GSH levels were found to be suppressed when the JNK pathway was inhibited (Fig. 9B); p62 expression was also depressed (Fig. 9D). Then we investigated whether the JNK pathway either affects cell survival or is involved in the ability of HT to prevent the *t*-BHP-induced loss of MMP. Cells were treated with SP600125 for 24 h, followed by treatment with 100 or 300 μM *t*-BHP for an additional 6 h, and MMP was measured. Treatment with SP600125 alone had no effect on MMP. Just as with LY294002 and BSO treatment, JNK inhibition greatly increased cell sensitivity and cells

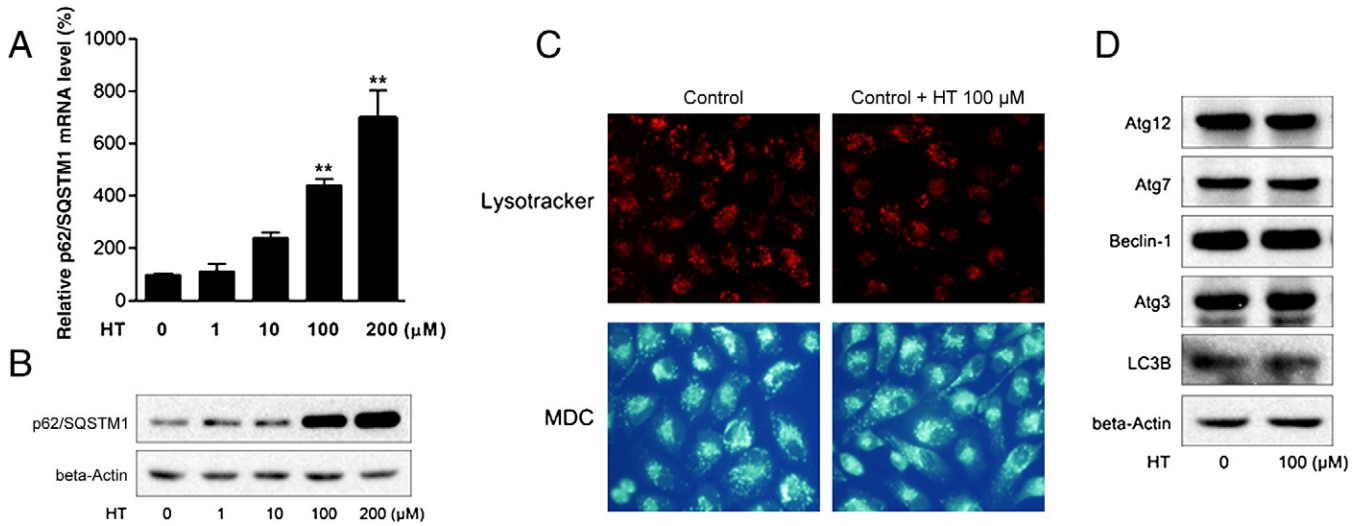

Fig. 8. HT induces p62 expression independent of autophagy dysfunction. ARPE-19 cells were treated with HT (1, 10, 100 or 200 μM) for 6 or 24 h. (A) p62 mRNA levels were examined after 6 h of treatment. (B) p62 protein levels were examined after 24-h treatment. Autophagy status of cells treated with 100 μM of HT was examined for 24 h. (C) Lysotracker and MDC staining were used to mark lysosomes and autophagosomes, respectively. (D) Autophagy-related proteins (Atg12, Atg7, Beclin-1, Atg3 and LC3B) were measured by Western blot. Values are means±S.E.M. from three separate experiments. *P<.05, **P<.01 versus related control.

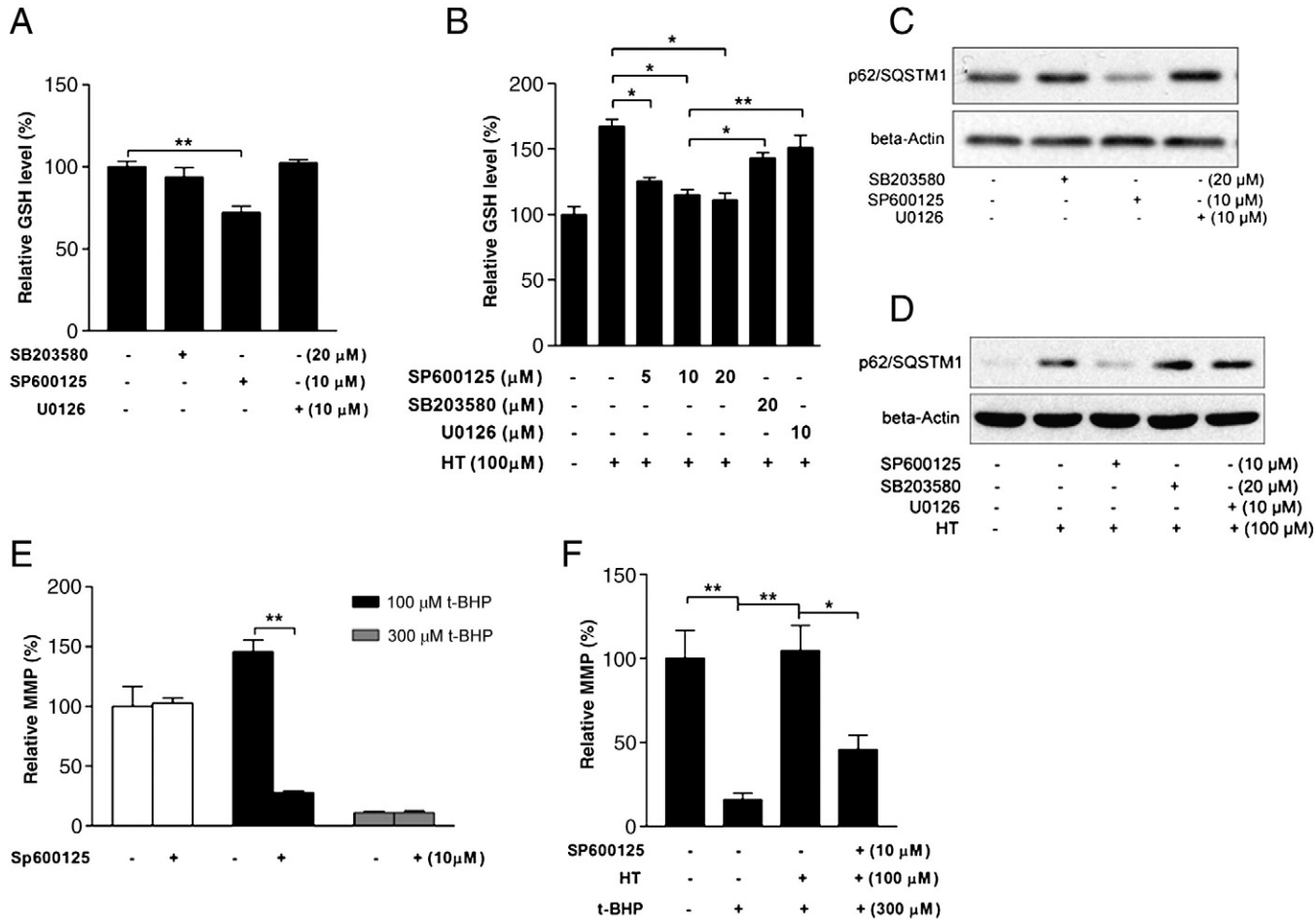

Fig. 9. Involvement of the JNK pathway in cell survival and induction of p62 and GSH. Cells were treated with 5, 10, 20 μM SP600125, 20 μM SB203580 and 10 μM U0126 with or without 100 μM HT for 24 h; GSH contents without HT (A) and with HT (B). p62 protein levels were measured without HT (C) and with HT (D). (E) MMP was measured in ARPE-19 cells pretreated with 10 μM SP600125 for 24 h followed by 100 or 300 μM *t*-BHP challenge for another 6 h. (F) MMP was measured in cells cultured for 24 h with 100 μM HT in the presence or absence of Sp600125, followed, where indicated by challenge, by 300 μM *t*-BHP for another 6 h. Values are means±S.E.M. from three separate experiments. *P<.05, **P<.01 versus related control.

showed significant MMP loss when challenged with 100 μM *t*-BHP (Fig. 9E). Cells were treated with 100 μM HT in the presence or absence of SP600125 for 24 h, challenged with *t*-BHP for another 6 h, followed by measurement of MMP. HT prevented the *t*-BHP-induced loss of MMP; JNK inhibition partly blocked HT's restorative action (Fig. 9F). Taken together, these results reveal that the JNK pathway plays an essential role in regulating p62 expression and GSH induction, two components of the mechanism by which HT protects against *t*-BHP-induced apoptosis.

4. Discussion

ARPE-19 cells have been widely used for research into age-related macular degeneration (AMD) pathogenesis, a process in which apoptotic or necrotic degeneration of RPE is believed to be involved [24,39–41]. In a previous study, we reported that HT can protect ARPE-19 cells from acrolein-induced necrotic cell death [24,25]. Because apoptosis is a major cause of RPE cell degeneration, in this study, we aimed to determine whether HT has protective effects against the apoptosis induced by *t*-BHP in ARPE-19 cells. We investigated how Nrf2 is involved in this protection. We measured MMP and viability of cells treated with *t*-BHP over a range of times and dosages and found that MMP was assuredly sensitive to *t*-BHP challenge. We used a 6-h treatment with 300 μM *t*-BHP as a standard for evaluating the protective effects of HT. Protein and lipid damage induced by oxidative stress is believed to be able to disrupt mitochondrial function, thereby leading to increased ROS levels and induction of apoptosis. However, in our study, ROS levels and activities of mitochondrial complexes I and II were not affected by a 6-h treatment with *t*-BHP; there was a slight increase in complex V activity, which might be an adaptive response to stress. Only after a 24-h challenge were ROS levels found to increase and mitochondrial complex activities to decrease. Apoptosis was observed to occur after only 6 h of treatment, indicating that it is not the outcome of oxidative damage. Since MMP was sensitive and almost 70% MMP loss occurred after 6 h of *t*-BHP treatment, we assume that direct MMP loss is the major cause of apoptosis.

Many researchers link MMP loss to GSH depletion by suggesting that MMP loss occurs downstream of the GSH loss, and GSH depletion may decrease MMP and increase the vulnerability of cells to apoptosis [42–50]. In the current study, we found that *t*-BHP could decrease GSH contents in a time- and dose-dependent manner, except that 100 μM *t*-BHP increased GSH contents after 6 h of treatment. It was interesting to find that a 6-h treatment with 100 μM *t*-BHP also increased MMP, indicating that MMP might be an effect associated with the increase in GSH. We then found that cells were sensitive to *t*-BHP challenge when GSH levels were depleted. Normally, 100 μM *t*-BHP treatment for 6 h increased MMP and had no effect on cell viability. In contrast, when GSH was depleted by BSO, 100 μM *t*-BHP

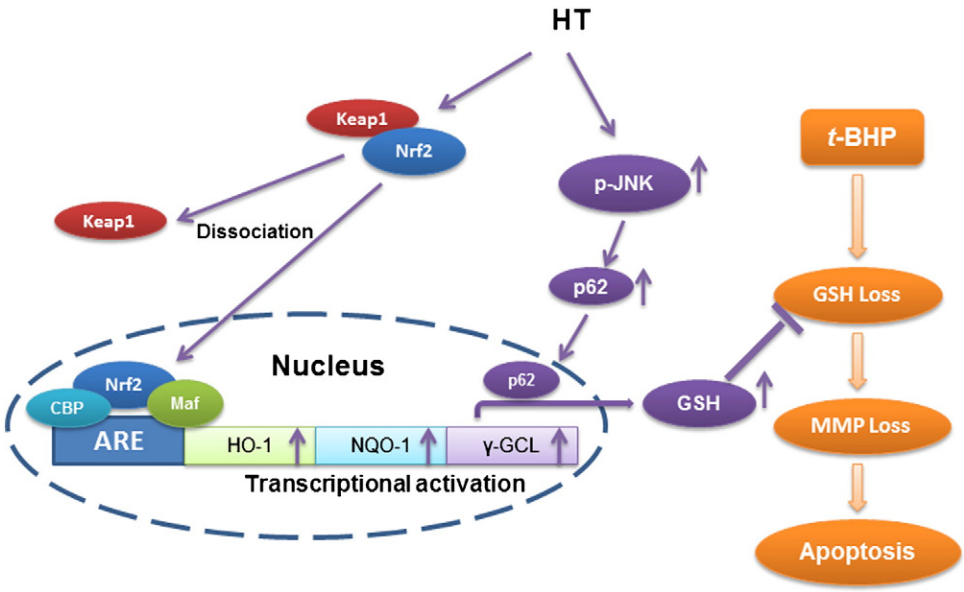

Fig. 10. Possible mechanism of HT protection against *t*-BHP induced cell apoptosis. *t*-BHP decreases GSH and therefore triggers MMP loss and apoptosis. HT induces GSH synthesis and prevents apoptosis. Nrf2 activation is required for HT protection to occur. JNK activation-induced p62 expression is required for Nrf2-induced GSH synthesis. On the other hand, Nrf2 activation-induced expression of either NQO-1 or HO-1 is independent of JNK activation. HT-induced activations of Akt, p38 and ERK kinases, though uninvolved in the induction of GSH synthesis, could lead to inhibition of apoptosis directly.

induced sharp losses in MMP and cell viability. Taken together, we conclude that GSH contents are critical for maintaining MMP and, consequentially, for preventing the apoptotic process.

Our results show that HT effectively protects ARPE-19 cells from *t*-BHP-induced reductions in MMP, oxygen consumption capacity, ATP levels and GSH contents, all of which are important for cell survival. HT treatment alone can increase GSH levels by about 50%, which we assume to be the most important contributor to HT's protective effect. In addition, HT alone could significantly increase mitochondrial oxygen consumption capacity and cellular GSH content except ATP content. We assumed that high oxygen consumption could cause higher ATP production, but GSH synthesis is an ATP-consuming process. This ATP consumption might cause no significant ATP increase after HT treatment. It has been reported that induction of GCLc and GCLm by Nrf2 activation regulates GSH production. We used siRNA specific to Nrf2 to confirm that HT induces GSH production via Nrf2 activation; four Nrf2 target genes, GCLc, GCLm, NQO-1 and HO-1, were measured as positive controls for Nrf2 activation. We then found that HT's protective effect was abolished when GSH production was inhibited by BSO, and this supports the notion that the GSH induced by HT via Nrf2 activation plays the key role in HT's protective effect against *t*-BHP-induced apoptosis (Fig. 10).

PI3 kinase has been characterized as an Nrf2 upstream regulator in many reports [34,51–53]. Studies show that Nrf2 activation can be efficiently inhibited by the specific PI3K inhibitor LY294002. In this study, we observed activation of the PI3K pathway by HT over time periods varying from 10 min to 2 h. To our surprise, HT could still activate Nrf2 when PI3K was inhibited by LY294002; congruously, HT also increased GSH production and exerted protective effects under these conditions. These results indicate that the activation of Nrf2 by HT is independent of PI3K. Thus, the pathway involved in the activation of Nrf2 still needs to be further investigated.

Recently, involvement of p62 in Nrf2 activation has been reported, which introduces a new mechanism that might improve understanding of HT's functionality. p62 can directly interact with Keap1, disrupt Keap1-Nrf2 binding and thus lead to accumulation of Nrf2 in the nucleus [20–22]. Little has been reported on p62 regulation. p62 has been found to accumulate in ubiquitin-containing aggregates when autophagy is disrupted in several model systems. The Terje Johansen group has just reported that p62 is also an Nrf2 target gene and is regulated by Nrf2, so that p62 can create a positive feedback loop in response to oxidative stress [23]. In our study, we found that HT increases p62 mRNA and protein levels dose dependently; we also found that regulation of p62 accumulation is not involved in autophagy. p62 expression and GSH content were decreased by JNK inhibitor SP600125 treatment. Moreover, induction by HT of either GSH or p62 was inhibited by the JNK inhibitor SP600125, and JNK activation was necessary for maintaining MMP in the presence of a *t*-BHP challenge. However, NQO-1 and HO-1 induction by HT was not inhibited by a JNK inhibitor (data not shown), which led us to consider Nrf2 regulation of p62 to be independent of JNK activation. We assume that p62 might be involved in GSH induction and thereby regulate HT's protective effects against a *t*-BHP challenge (Fig. 10). However, this hypothesis needs to be investigated further.

In conclusion, these results strongly suggest that GSH reduction by a *t*-BHP challenge can induce MMP loss, which in turn might cause ARPE-19 cells to undergo apoptosis directly. HT is an effective Nrf2 inducer and increases GSH levels via Nrf2 activation, thereby protecting ARPE-19 cells from *t*-BHP-induced apoptosis. Moreover, instead of the PI3K pathway, the JNK pathway was found to be involved in GSH and p62 induction. For the first time, we consider p62 to be a regulator involved in GSH production, a function that needs further confirmation. Regardless, presence of p62 in the Nrf2 system reveals a new aspect of the cellular antioxidant system and also provides potential targets for therapeutic treatments of diseases such as AMD that involve retinal degeneration.

Acknowledgments

We thank Dr. Edward Sharman at the University of California, Irvine, for reading and editing this manuscript. We thank Dr. Yue Xiong at Lineberger Cancer Center, University of North Carolina, for generosity of the gift of pCDNA3-Myc3-Nrf2-FLAG. This study was partly supported by the National Natural Science Foundation of China (Key Program, No. 30930105), DSM Nutritional Products Ltd. and Xi'an Jiaotong University (985 and 211 projects).

References

[1] Moi P, Chan K, Asunis I, Cao A, Kan YW. Isolation of NF-E2-related factor 2 (Nrf2), a NF-E2-like basic leucine zipper transcriptional activator that binds to the tandem NF-E2/AP1 repeat of the beta-globin locus control region. Proc Natl Acad Sci U S A 1994;91:9926–30.

[2] Li W, Kong AN. Molecular mechanisms of Nrf2-mediated antioxidant response. Mol Carcinog 2009;48:91–104.

[3] Nguyen T, Nioi P, Pickett CB. The Nrf2-antioxidant response element signaling pathway and its activation by oxidative stress. J Biol Chem 2009;284: 13291–5.

[4] Itoh K, Wakabayashi N, Katoh Y, Ishii T, Igarashi K, Engel JD, et al. Keap1 represses nuclear activation of antioxidant responsive elements by Nrf2 through binding to the amino-terminal Neh2 domain. Genes Dev 1999;13:76–86.

[5] Kobayashi A, Kang MI, Okawa H, Ohtsuji M, Zenke Y, Chiba T, et al. Oxidative stress sensor Keap1 functions as an adaptor for Cul3-based E3 ligase to regulate proteasomal degradation of Nrf2. Mol Cell Biol 2004;24:7130–9.

[6] Sekhar KR, Rachakonda G, Freeman ML. Cysteine-based regulation of the CUL3 adaptor protein Keap1. Toxicol Appl Pharmacol 2010;244:21–6.

[7] Furukawa M, Xiong Y. BTB protein Keap1 targets antioxidant transcription factor Nrf2 for ubiquitination by the Cullin 3-Roc1 ligase. Mol Cell Biol 2005;25: 162–71.

[8] Itoh K, Chiba T, Takahashi S, Ishii T, Igarashi K, Katoh Y, et al. An Nrf2/small Maf heterodimer mediates the induction of phase II detoxifying enzyme genes through antioxidant response elements. Biochem Biophys Res Commun 1997;236:313–22.

[9] Jarmi T, Agarwal A. Heme oxygenase and renal disease. Curr Hypertens Rep 2009;11:56–62.

[10] Kobayashi M, Yamamoto M. Nrf2-Keap1 regulation of cellular defense mechanisms against electrophiles and reactive oxygen species. Adv Enzyme Regul 2006;46:113–40.

[11] Edgren M, Revesz L, Larsson A. Induction and repair of single-strand DNA breaks after X-irradiation of human fibroblasts deficient in glutathione. Int J Radiat Biol Relat Stud Phys Chem Med 1981;40:355–63.

[12] Working PK, Smith-Oliver T, White RD, Butterworth BE. Induction of DNA repair in rat spermatocytes and hepatocytes by 1,2-dibromoethane: the role of glutathione conjugation. Carcinogenesis 1986;7:467–72.

[13] Kosower NS, Vanderhoff GA, Kosower EM. Glutathione. 8. The effects of glutathione disulfide on initiation of protein synthesis. Biochim Biophys Acta 1972;272:623–37.

[14] Padgett CM, Whorton AR. Glutathione redox cycle regulates nitric oxide-mediated glyceraldehyde-3-phosphate dehydrogenase inhibition. Am J Physiol 1997;272: C99–108.

[15] Fidelus RK, Ginouves P, Lawrence D, Tsan MF. Modulation of intracellular glutathione concentrations alters lymphocyte activation and proliferation. Exp Cell Res 1987;170:269–75.

[16] Hamilos DL, Zelarney P, Mascali JJ. Lymphocyte proliferation in glutathione-depleted lymphocytes: direct relationship between glutathione availability and the proliferative response. Immunopharmacology 1989;18:223–35.

[17] Joung I, Strominger JL, Shin J. Molecular cloning of a phosphotyrosine-independent ligand of the p56lck SH2 domain. Proc Natl Acad Sci U S A 1996;93:5991–5.

[18] Sanchez P, De Carcer G, Sandoval IV, Moscat J, Diaz-Meco MT. Localization of atypical protein kinase C isoforms into lysosome-targeted endosomes through interaction with p62. Mol Cell Biol 1998;18:3069–80.

[19] Puls A, Schmidt S, Grawe F, Stabel S. Interaction of protein kinase C zeta with ZIP, a novel protein kinase C-binding protein. Proc Natl Acad Sci U S A 1997;94: 6191–6.

[20] Fan W, Tang Z, Chen D, Moughon D, Ding X, Chen S, et al. Keap1 facilitates p62-mediated ubiquitin aggregate clearance via autophagy. Autophagy 2010;6.

[21] Lau A, Wang XJ, Zhao F, Villeneuve NF, Wu T, Jiang T, et al. A noncanonical mechanism of Nrf2 activation by autophagy deficiency: direct interaction between Keap1 and p62. Mol Cell Biol 2010;30:3275–85.

[22] Komatsu M, Kurokawa H, Waguri S, Taguchi K, Kobayashi A, Ichimura Y, et al. The selective autophagy substrate p62 activates the stress responsive transcription factor Nrf2 through inactivation of Keap1. Nat Cell Biol 2010;12:213–23.

[23] Jain A, Lamark T, Sjottem E, Larsen KB, Awuh JA, Overvatn A, et al. p62/SQSTM1 is a target gene for transcription factor NRF2 and creates a positive feedback loop by inducing antioxidant response element-driven gene transcription. J Biol Chem 2010;285:22576–91.

[24] Liu Z, Sun L, Zhu L, Jia X, Li X, Jia H, et al. Hydroxytyrosol protects retinal pigment epithelial cells from acrolein-induced oxidative stress and mitochondrial dysfunction. J Neurochem 2007;103:2690–700.

[25] Zhu L, Liu Z, Feng Z, Hao J, Shen W, Li X, et al. Hydroxytyrosol protects against oxidative damage by simultaneous activation of mitochondrial biogenesis and phase II detoxifying enzyme systems in retinal pigment epithelial cells. J Nutr Biochem 2010;21:1089–98.

[26] Jia L, Liu Z, Sun L, Miller SS, Ames BN, Cotman CW, et al. Acrolein, a toxicant in cigarette smoke, causes oxidative damage and mitochondrial dysfunction in RPE cells: protection by (R)-alpha-lipoic acid. Invest Ophthalmol Vis Sci 2007;48: 339–48.

[27] Philp NJ, Wang D, Yoon H, Hjelmeland LM. Polarized expression of monocarboxylate transporters in human retinal pigment epithelium and ARPE-19 cells. Invest Ophthalmol Vis Sci 2003;44:1716–21.

[28] Sun L, Luo C, Long J, Wei D, Liu J. Acrolein is a mitochondrial toxin: effects on respiratory function and enzyme activities in isolated rat liver mitochondria. Mitochondrion 2006;6:136–42.

[29] Long J, Wang X, Gao H, Liu Z, Liu C, Miao M, et al. Malonaldehyde acts as a mitochondrial toxin: inhibitory effects on respiratory function and enzyme activities in isolated rat liver mitochondria. Life Sci 2006;79:1466–72.

[30] Li X, Liu Z, Luo C, Jia H, Sun L, Hou B, et al. Lipoamide protects retinal pigment epithelial cells from oxidative stress and mitochondrial dysfunction. Free Radic Biol Med 2008;44:1465–74.

[31] LeBel CP, Ischiropoulos H, Bondy SC. Evaluation of the probe 2′,7′-dichlorofluorescin as an indicator of reactive oxygen species formation and oxidative stress. Chem Res Toxicol 1992;5:227–31.

[32] White CC, Viernes H, Krejsa CM, Botta D, Kavanagh TJ. Fluorescence-based microtiter plate assay for glutamate-cysteine ligase activity. Anal Biochem 2003;318:175–80.

[33] Li J, Johnson D, Calkins M, Wright L, Svendsen C, Johnson J. Stabilization of Nrf2 by tBHQ confers protection against oxidative stress-induced cell death in human neural stem cells. Toxicol Sci 2005;83:313–28.

[34] Wang L, Chen Y, Sternberg P, Cai J. Essential roles of the PI3 kinase/Akt pathway in regulating Nrf2-dependent antioxidant functions in the RPE. Invest Ophthalmol Vis Sci 2008;49:1671–8.

[35] Okouchi M, Okayama N, Alexander JS, Aw TY. NRF2-dependent glutamate-L-cysteine ligase catalytic subunit expression mediates insulin protection against hyperglycemia- induced brain endothelial cell apoptosis. Curr Neurovasc Res 2006;3:249–61.

[36] Langston W, Circu ML, Aw TY. Insulin stimulation of gamma-glutamylcysteine ligase catalytic subunit expression increases endothelial GSH during oxidative stress: influence of low glucose. Free Radic Biol Med 2008;45:1591–9.

[37] Faghiri Z, Bazan NG. PI3K/Akt and mTOR/p70S6K pathways mediate neuroprotectin D1-induced retinal pigment epithelial cell survival during oxidative stress-induced apoptosis. Exp Eye Res 2010;90:718–25.

[38] Komatsu M, Waguri S, Koike M, Sou YS, Ueno T, Hara T, et al. Homeostatic levels of p62 control cytoplasmic inclusion body formation in autophagy-deficient mice. Cell 2007;131:1149–63.

[39] Hinton DR, He S, Lopez PF. Apoptosis in surgically excised choroidal neovascular membranes in age-related macular degeneration. Arch Ophthalmol 1998;116: 203–9.

[40] Dunaief JL, Dentchev T, Ying GS, Milam AH. The role of apoptosis in age-related macular degeneration. Arch Ophthalmol 2002;120:1435–42.

[41] Feng Z, Liu Z, Li X, Jia H, Sun L, Tian C, et al. alpha-Tocopherol is an effective phase II enzyme inducer: protective effects on acrolein-induced oxidative stress and mitochondrial dysfunction in human retinal pigment epithelial cells. J Nutr Biochem 2010;21:1222–31.

[42] Han YH, Kim SH, Kim SZ, Park WH. Apoptosis in arsenic trioxide-treated Calu-6 lung cells is correlated with the depletion of GSH levels rather than the changes of ROS levels. J Cell Biochem 2008;104:862–78.

[43] Han YH, Yang YM, Kim SZ, Park WH. Attenuation of MG132-induced HeLa cell death by *N*-acetyl cysteine via reducing reactive oxygen species and preventing glutathione depletion. Anticancer Res 2010;30:2107–12.

[44] Swamy SM, Huat BT. Intracellular glutathione depletion and reactive oxygen species generation are important in alpha-hederin-induced apoptosis of P388 cells. Mol Cell Biochem 2003;245:127–39.

[45] Bojes HK, Feng X, Kehrer JP, Cohen GM. Apoptosis in hematopoietic cells (FL5.12) caused by interleukin-3 withdrawal: relationship to caspase activity and the loss of glutathione. Cell Death Differ 1999;6:61–70.

[46] Backway KL, McCulloch EA, Chow S, Hedley DW. Relationships between the mitochondrial permeability transition and oxidative stress during ara-C toxicity. Cancer Res 1997;57:2446–51.

[47] Han YH, Moon HJ, You BR, Park WH. Propyl gallate inhibits the growth of calf pulmonary arterial endothelial cells via glutathione depletion. Toxicol In Vitro 2010;24:1183–9.

[48] Han YH, Park WH. Pyrogallol-induced As4.1 juxtaglomerular cell death is attenuated by MAPK inhibitors via preventing GSH depletion. Arch Toxicol 2010;84:631–40.

[49] Chiou JF, Wang YH, Jou MJ, Liu TZ, Shiau CY. Verteporfin-photoinduced apoptosis in HepG2 cells mediated by reactive oxygen and nitrogen species intermediates. Free Radic Res 2010;44:155–70.

[50] Han YH, Park WH. The effects of MAPK inhibitors on antimycin A-treated Calu-6 lung cancer cells in relation to cell growth, reactive oxygen species, and glutathione. Mol Cell Biochem 2010;333:211–9.

[51] Lee JM, Hanson JM, Chu WA, Johnson JA. Phosphatidylinositol 3-kinase, not extracellular signal-regulated kinase, regulates activation of the antioxidant-responsive element in IMR-32 human neuroblastoma cells. J Biol Chem 2001;276: 20011–6.

[52] Johnson DA, Andrews GK, Xu W, Johnson JA. Activation of the antioxidant response element in primary cortical neuronal cultures derived from transgenic reporter mice. J Neurochem 2002;81:1233–41.

[53] Patel R, Maru G. Polymeric black tea polyphenols induce phase II enzymes via Nrf2 in mouse liver and lungs. Free Radic Biol Med 2008;44:1897–911.